NANO LETTERS

2008
Vol. 8, No. 3
866-871

Bending Membranes on Demand: Fluid Phospholipid Bilayers on Topographically Deformable Substrates

Babak Sanii,[†] Andreia Michelle Smith,[‡] Ravichandra Butti,[†] Adrian M. Brozell,[‡] and Atul N. Parikh*[,†,‡]

Department of Applied Science and, Biophysics Graduate Group, University of California, Davis, California 95616

Received November 26, 2007; Revised Manuscript Received January 25, 2008

ABSTRACT

We combine hierarchical surface wrinkling of elastomers with lipid membrane deposition techniques to dynamically template complex three-dimensional topographies onto supported lipid bilayers. The real-time introduction of corresponding nano- to micrometer scale curvatures triggers spatially periodic, elastic bending of the bilayer, accompanied by molecular-level reorganizations. This ability to dynamically impose curvatures on supported bilayers and the ensuing re-equilibration promises fundamental material and biophysical investigations of curvature-dependent, static heterogeneities and dynamic reorganizations pervasive in biological membranes.

Membrane curvature, static and dynamic, is not a passive consequence of cellular activity. Rather it represents an active conformational switch to spatially regulate many cell−surface interactions and intracellular trafficking. Several essential biological functions, including vesicular budding, viral interactions, mitosis, and membrane fusion, proceed via structural intermediates that display well-defined transient curvatures.[1–3] Inside the cell, quasistatic curvatures also exist in microvilli and as folded membranes in many organelles (e.g., cilia and mitochondria). Living cells stabilize (or modulate) their local membrane curvatures by concentrating or dynamically recruiting molecules with intrinsic curvatures (e.g., lipids, membrane proteins, and amphiphilic helical peptides) or via time-dependent external scaffolding mechanisms including cytoskeletal (re)polymerization or motor protein activity.[3] Among in vitro model membranes, giant vesicles have also been shown to reconstitute local and dynamic variations in curvature.[4,5] For instance, high concentrations of curvature-sensitive molecules and applications of external forces (e.g., tension and shear) deform liposomes to form tethers and tubules.[6] Recently, using relatively simple lipid mixtures, chemical phase separations of lipids within giant vesicles have been shown to produce complex topologies characterized by budding and fission at the phase boundaries of coexisting domains.[7,8] In this same vein, static curvatures imposed on planar bilayers using supported membrane configurations have also been shown to result in spatial redistributions and domain formation.[9,10]

Independently, methods are emerging in the field of soft materials to controllably induce periodic surface topographic curvatures via structural failures and mechanical instabilities.[11–14] These approaches allow for the design of predictable patterns of surface topographies such as buckles, bristles, and wrinkles in simple, convenient, nonlithographic, and cost-effective ways. For instance, releasing stretched poly(dimethyl)siloxane (PDMS) elastomers after surface oxidation produces multiple nested orders of periodic curvatures over macroscopic areas of the surface. Properties of the surface wrinkles (e.g., radii of curvature and wavelengths) are tunable and reversible depending on the conditions used for surface oxidation, the manner in which the elastomer is stretched (e.g., linear anisotropic, radial, etc.), and the rate at which the stretch configuration is released following oxidation.[15–17]

In the work reported here, we establish that single supported phospholipid bilayers formed at the interfaces between deformable, oxidized PDMS elastomers and aqueous phases are coupled to the substrate topography. Real-time variations of substrate topography trigger spatially patterned mesoscale restructuring of the bilayer accompanied by curvature-dependent spatial reorganization of membrane molecules. This ability to dynamically impose curvatures on supported bilayers and the attendant re-equilibration promises fundamental studies of a range of curvature-induced dynamic reorganizations and their functional consequences in a massively parallel fashion. Together, these observations

* Corresponding author. E-mail: anparikh@ucdavis.edu. Address: 3001 EU III, University of California at Davis, One Shields Avenue, Davis, California, 95616.
† Department of Applied Science, University of California.
‡ Biophysics Graduate Group, University of California.

10.1021/nl073085b CCC: $40.75
Published on Web 02/14/2008

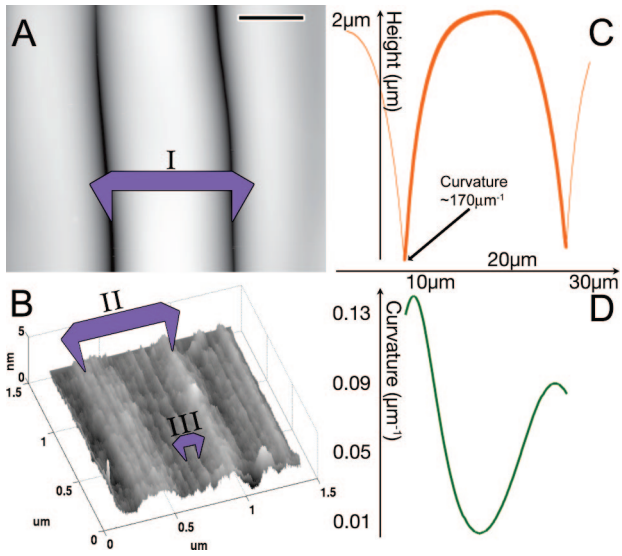

Figure 1. Hierarchical, wrinkled substrates. (A,B) AFM scans of a wrinkled substrate revealing its hierarchical surface. The distances noted by roman numerals are (I) 19 μm, (II) 0.6 μm, and (III) 80 nm. (B) was locally flattened with a 7th-order polynomial, and the scale bar in (A) represents 10 μm. (C) Trace of the AFM-measured heights associated with the largest order of wrinkling (achieved by local smoothing). The estimated curvature in the region between wrinkles (from nonsmoothed AFM scans, see Supporting Information) is noted. (D) Trace of the curvatures[36] associated with the single period of wrinkling shown in (C), excluding the region between the wrinkles.

suggest a mechanical, macroscopic knob to control the molecular interactions of membranes. Because patterns of curvatures can stabilize heterogeneous distribution of molecules within fluid membranes, these model systems may also provide a generic means to create sustained molecular gradients and carry out spatial separations of membrane-compatible amphiphiles.

We begin with the preparation of topographically deformable elastomers by adapting a previously reported method.[12] Briefly, planar PDMS is uniaxially stretched (Supporting Information) by ~30–50% and its surface exposed to ozone-producing, short-wavelength UV radiation (184–257 nm) for ~45 min. The treatment is known to oxidatively remove backbone methyl groups and promote further cross-linking of silanols, thus forming a dense silica-like skin (ox-PDMS ~5 nm thick, and ~50% the silica density of glass).[18] Subsequent rapid release of the strain results in a periodic pattern of nested 1D curvatures, which span at least three distinct generations, in a direction perpendicular to that of the initial stretch (Figure 1). The largest period so produced here is ~18 μm, and the smallest measured period, embedded hierarchically, is ~80 nm. This nested hierarchy of wrinkles form because of the mismatch in equilibrium strains of the skin and the underlying elastic substrate.[12] While still in the stretched configuration, the newly formed skin is equilibrated while the bulk remains under tensile stress. Removing the stretch exerts a compressive strain on the skin that gives rise to a bending-dominated deformation, forming the smallest wavelength wrinkles. The saturation of the amplitude of these wrinkles leads to higher-order wrinkles determined by the precise competition between the bending-dominated deformation of the skin and the stretching-dominated response of the underlying PDMS.[12] Thus by controlling the initial extension and the rate of release, a variety of surface structures and length scales can be produced.[19] Here we examine 1D hierarchical wrinkles, but radial, hexagonal, and other geometries that generate 2D curvatures over many scales of order are also readily achieved.

The ability of phospholipid bilayers to self-assemble in a topology prescribed by the curvature patterns of the underlying wrinkled elastomer is first established using both vesicle fusion and lipid spreading methods. For vesicle fusion, an aqueous dispersion of small unilamellar vesicles (SUVs, hydrodynamic diameter of~110 nm) consisting of a fluid phospholipid, namely 1-palmitoyl-2-oleoyl-*sn*-glycero-3-phosphocholine (POPC, transition temperature, T_m, −2 °C) doped with a small concentration (1 mol) of fluorescent Texas Red 1,2-dihexadecanoyl-*sn*-glycero-3-phosphoethanolamine triethylammonium salt (TR-DHPE) is incubated with freshly wrinkled, ox-PDMS elastomer (Supporting Information).[20] Wide-area epifluorescence microscopy reveals a homogeneous fluorescence emission interrupted by enhanced parallel streaks of greater fluorescence emission (Figure 2A). Comparable results were obtained using lipid spreading[21] (Supporting Information). In all cases, the brighter streaks correspond directly to longitudinal features in a bright-field transmission image of the sample. Large silica beads (5 μm diameter) introduced into the aqueous phase and allowed to gravitationally settle colocalize with these features, establishing them as the grooves of the wrinkles (Figure 2B). That the membrane formed represents a single bilayer is confirmed in a control experiment: exposure of a membrane impermeable quenching agent (anti-Texas Red, rabbig IgG purchased from Molecular Probes) to membranes formed on wrinkled substrates reduces the fluorescence intensity by the same fraction as when exposed to a single bilayer on flat ox-PDMS (Supporting Information). The enhanced fluorescence intensity near the grooves is consistent with a greater lipid density projected onto the image plane by the curved substrate topography. This suggests that the bilayer bends in concert with the ox-PDMS. Fluorescence enhancement alone, however, cannot be used to quantify the extent of membrane bending because of the strong dependence of fluorescence emission on the changing lipid microenvironment as the bilayer topography is curved.

The long-range lateral mobility of phospholipids in bilayers is crucial for higher-order curvature-dependent self-assembly (e.g., phase segregation) to occur within the membrane environment. To determine that the undulating bilayer supported on wrinkled ox-PDMS is fluid over macroscopic areas, we adapted a simple microscopy-based, two-dimensional (2D) fluorescence recovery after photobleaching (FRAP) experiment.[22] Furthermore, because the curvatures are arrayed in 1D and the diffusion follows along a 2D Brownian path, the precise trajectory of the fluorescence recovery process can also be used to determine the extent of membrane bending and/or any curvature-dependent, spatial variations in molecular diffusivities. We first produced a circular photobleached spot (of diminished Gaussian distri-

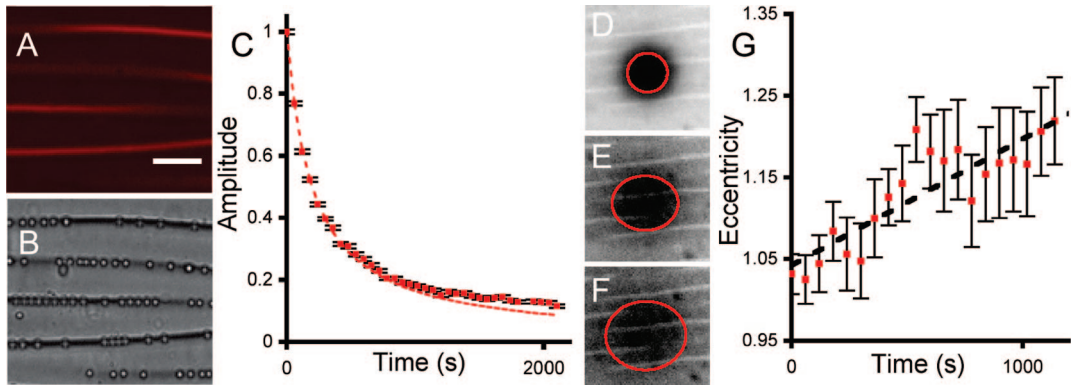

Figure 2. Phospholipid bilayers on wrinkled elastomers. (A,B) Wide-area epifluorescence (A) and bright-field optical transmission (B) images of a POPC bilayer (doped with 1 mol % Texas Red DHPE) on a prewrinkled PDMS elastomer. The image in B is acquired after 5 μm beads are allowed to settle onto the bilayer. The white bar scales to 50 μm. (C) Normalized Gaussian amplitude of a bleached FRAP spot's intensity depression as a function of time, showing fluid recovery. Dashed line is a fit to the expected recovery profile (see Supporting Information for analysis). (D−F) Selected frames from a sequence of fluorescence images showing recovery dynamics of a circular spot photobleached into a POPC bilayer (doped with 1 mol % TR-DHPE) deposited on the wrinkled ox-PDMS substrate shown in Figure 1, at representative time intervals (t = 0, 600, and 1020 s after photobleaching). The red trace is an ellipse fit to the spot edges. Images scale to 112 × 112 μm^2. (G) Temporal evolution of eccentricity of the photobleached spot in panels (D−F).

bution of intensity, spanning multiple corrugations) by exposing the bilayer to an intense beam of light at the fluorophore's excitation wavelength. The intensity recovery of the bleached spot establishes substantial lateral fluidity of the bilayer (Figure 2C). A quantitative analysis reveals an axially averaged diffusion coefficient of 1.2 ± 0.2 μm^2/s (Supporting Information), in good agreement with lipid bilayers on glass[23] and flat ox-PDMS substrates[24] (1–5 μm^2/s). Further examination of the time-lapse movie of the fluorescence recovery dynamics reveals that the initial circular morphology of the photobleached spot transitions into an elliptical one (Figure 2D−F). The observed ellipse is oriented with its major axis aligned parallel to the grooves of the wrinkles. Because the projection of a 2D diffusing Gaussian shape (profile of the photobleached spot) over a topography curved along a fixed dimension also evolves into a similarly oriented ellipse (analytically derived in Supporting Information), it appears reasonable that the membrane must adhere to the substrate topography.

The evolution of the photobleached spot from an initial circular shape to an elliptical one (prior to complete recovery producing homogeneous fluorescence field) can be further quantified in terms of spot eccentricity. Defined as the ratio of the major to the minor axes of the photobleached spot, it provides a measure of apparent disparity in spot recovery along the two principle axes, namely parallel and perpendicular to the grooves. This anisotropy in spot evolution originates from the fact that the diffusive path perpendicular to the grooves is three-dimensionally distributed and longer than the planar path parallel to the grooves. Thus, its two-dimensional projection, such as that seen in the FRAP experiments, estimates the extent of membrane's out-of-plane bending, presumably along the surface wrinkles. We measure the time-dependent fluorescence spot eccentricity by thresholding each frame at the 50% value between the mean intensity at the center of the bleached spot and the mean intensity at an arbitrary region farther away from the spot (>3 Gaussian spreads). A map connecting all the pixels of each class highlights the periphery of the blurring spot. The perimeter of the highlight is then fit to an ellipse using a standard least-squares fitting algorithm[25] (see Supporting Information for a video showing the fitting) and the properties of the ellipse are recorded. The ratio of major to minor axes of the fitted ellipse is taken as the spot eccentricity and plotted as a function of time following photobleaching. The uncertainties in the measurements of the principle axes of the fitted ellipse serve as the primary source of our measurement errors. Note also that, at longer times when spot ellipticity reflects the quantitative differences in diffusive paths along the major and the minor axis, the net diffusion begins to homogenize the fluorescence field, making it difficult to accurately threshold the shape of the spot.

The time-dependent growth of eccentricities in FRAP spots (Figure 2G) shows a monotonic growth. The corresponding images in Figure 2C−F also confirm that, during this period, the spot also becomes increasingly less well-defined. This monotonic growth in spot eccentricity consistently reflects the disparity in the projected translational mobility of the fluorescent probe (e.g., Texas-red DHPE) along the two principle axes. This displarity must approach an asymptotic value determined by the extent of membrane bending along the substrate wrinkles before fluorescence homogenization. In the time scales of our measurement, we do not observe the asymptote. The highest value of the observed eccentricity (e = 1.22 ± 0.05) affords some comparison with the substrate topography. If the membrane precisely followed the curvature of only the largest wrinkle period, we expect an asymptotic eccentricity of ~1.04. This value is obtained by taking the ratio of surface path length afford by the wrinkled substrate and as characterized by AFM scan of the same region (Figure 1) to the flat projected image plane (see Supporting Information for details). In contrast, complete epitaxy between the bilayer and the substrate topography, including all measurable higher-order wrinkles, should produce an asymptotic eccentricity of ~2.54. Our observed limiting value of 1.22 ± 0.05 suggests that the membrane

follows at least the largest wrinkle period, albeit this simple analysis does not preclude some adherence to higher-order wrinkles. Note also that the membrane's adherence to high curvatures may induce local changes in lipid packing in the vicinity of grooves, thereby perturbing translational diffusivity of probe lipids perpendicular to the grooves. This further complicates the analysis of the evolution of spot eccentricity of the recovering photobleached spot in accurately quantitating membrane bending.

Indeed, perfect epitaxy, involving the ability of the membrane to bend along the sharpest substrate curvatures ($\sim$0.17 nm^{-1}, see Supporting Information), is unlikely for at least two reasons. First, the surface roughness created by the smallest wrinkles may influence the membrane's ability to adhere to the substrate. A recent theoretical study based on continuum descriptions suggest that small surface topographic periodicities (<31 m) can considerably decrease (by more than >10%) membrane adhesion energy.[26] Moreover, the properties of the intervening water layer between the substrate the bilayer may also be locally different, altering bilayer formation at high curvatures. Second, at the highest curvatures, membrane bending energy becomes significant, competing with surface adhesion energy.[27] Systematic studies correlating bilayer compliance with substrate topographic roughness, its effects on lipid packing and probe diffusivities, and properties of interfacial water are needed to fully quantity the bilayer epitaxy to substrates displaying nanometer scale topographic undulations.

Curvatures in living systems are highly dynamic. During essential cellular processes such as growth, division, and motility, cellular membranes undergo dramatic conformational changes. Such dynamic membrane remodeling proceeds via incorporation of curvature-sensitive lipids (compositional dynamics in membranes) and via interactions with curvature-generating and curvature-sensing proteins. To test if flexible PDMS (together with its inflexible silica skins) can be used as a topographically dynamic substrate that induces such remodeling in the lipid bilayer supported on it, we carried out a simple proof-of-concept experiment. Briefly, a still-stretched ($\sim$30%) flat PDMS elastomer is subject to a typical UVO treatment (see above) to generate an ox-PDMS surface. In two parallel experiments, SUVs of dipalmitoyl-*sn*-glycero-3-phosphocholine (DPPC, T_m 41 °C) and POPC (T_m −2 °C) are fused to the sample at temperatures above their respective T_m values and then allowed to equilibrate at room temperature ($\sim$24 °C), all while the PDMS is still stretched. Epifluorescence images reveal a homogeneous bilayer for each sample, consistent with the formation of a planar supported bilayer on flattened, stretched ox-PDMS. A circular spot ($\sim$650 μm diameter) spanning multiple topographic corrugations is then photobleached into both DPPC and POPC specimens. The stretch is released and, as expected, the substrate deforms in two parallel modes: (1) the bulk PDMS tries to laterally restore its original shape by compressing in the stretched direction and elongating in the perpendicular one determined by the PDMS's Poisson ratio of $\sim$0.5, and (2) the mismatch in the equilibrium strains of the surface skin and the bulk PDMS produces periodic

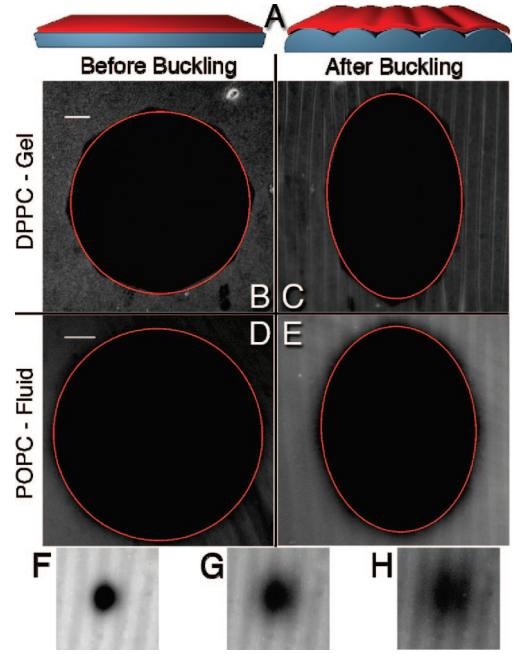

Figure 3. Active membrane remodeling via surface wrinkling. (A) Cartoon depiction of a lipid bilayer (red) supported on stretched planar ox-PDMS before (left) and after (right) the stretch is released. (B−E) Representative epifluorescence images showing macroscopic membrane remodeling after release of the mechanical stretch. Left column: circular spots bleached into membranes deposited onto stretched ox-PDMS before release. Right column: spots after the stretch was released and the substrate has wrinkled. Top row: DPPC lipids in a gel state. Bottom row: POPC lipids in a fluid state. The white bars scale to 100 μm and are consistent across rows, and red traces are least-squares fits of ellipses to the bleached areas. (F−H) Recovery of a spot photobleached into a lipid membrane after remodeling via substrate wrinkling. The images are 30, 400, and 1100 s after bleaching, respectively, and scale to 65 μm on a side.

out-of-plane wrinkles, confirmed by bright-field microscopy. Simultaneously, a dramatic transformation in the shape of the fluorescence spot is observed for both POPC and DPPC bilayers: in both cases, the initial circular spot transforms into an elliptical one, with the minor axis in the direction of the released stretch (see Figure 3). Both bleached spots recover when heated to above their respective melting temperatures, indicating that the membranes remain laterally contiguous though the wrinkling transition. FRAP analysis of POPC membranes that have undergone a wrinkling transition indicates an azimuthally averaged diffusion coefficient of 1.7 $\pm$ 0.4 μm^2/s (see Figure 3F−H). The recovery was anisotropic, consistent with membranes deposited on prewrinkled substrates. Together, these results establish that substrate deformation and wrinkling remodel membrane bilayers in the fluid (POPC at 24 °C) and, more remarkably, in the gel (DPPC at 24 °C) phase.

We postulate that this membrane remodeling is driven primarily by the dominance of substrate−membrane adhesion energy over the bending energy penalties that the membrane must incur. To determine the degree to which substrate curvature is templated into the bilayer, we compare the lengths of the spots along the stretched axes before and after wrinkling. Assuming that the glassy skin is relatively incompressible (its

Young's modulus is ~3600 times greater than that of PDMS), we determine that the 1D curved path lengths may be as much as 1.37 and 1.33 times longer than the projected ones for fluid- and gel-phase membranes, respectively. This agrees well with the elliptical recovery observed on the static wrinkles (see above) and furnishes strong evidence of bilayer−substrate epitaxy. Does the mesoscale membrane remodeling (induced by underlying substrate topography) give rise to molecular reorganizations within fluid lipid bilayers? Such reorganizations are pervasive in cellular membranes producing sustained (or transient) molecular heterogeneity and concentration gradients. It has been variously argued that shape-induced compositional (and hence structural) heterogeneities in membranes provide microenvironments or functional hot-spots needed to concentrate curvature-dependent functions.[10,28,29] Bilayers on reconfigurable PDMS substrates are particularly suitable to addressing the type of molecular rearrangements, which occur in response to spatial (and temporal) variations in membrane curvature. To demonstrate this capability, we first deposit a single 1,2-dimyristoyl-*sn*-glycero-3-phosphocholine (DMPC, T_m 24 °C) bilayer from SUVs. The bilayer is doped with small amounts of two fluorescent lipid analogues, namely DiI-C_{18} (1,1′-dioctadecyl-3,3,3′,3′-tetramethylindocarbocyanine perchlorate, 1 mol %) and BODIPY-FL-C_{12} (4,4-difluoro-5,7-dimethyl-4-bora-3a,4a-diaza-*s*-indacene-3-dodecanoic acid, 3 mol %) with notably different phase sensitivities and emission spectra. The long-chain DiI-C_{18} lipid analogue, consisting of a large indocarbocyanine headgroup and two octadecyl chains, inserts into the membrane with its headgroup roughly perpendicular to the plane of the bilayer. The slightly longer length of the probe alkyl chains (C_{18}) compared to those of the host DMPC acyl chains (C_{14}) results in a preferential partitioning of the probe into ordered, gel-like dense states of DMPC.[30–32] In contrast, the BODIPY derivatized fatty acid, consisting of a small carboxylic acid headgroup and a single, shorter aliphatic chain (C_{12}), is largely insensitive to the local amphiphilic environment and partitions into DMPC bilayers without a measurable preference for the local lipid density of the bilayer.[21] The warm fluid bilayer is then gradually cooled to below the T_m of DMPC, and spatial redistributions of the two-dyes are probed in real time using temperature-programmed fluorescence microscopy measurements.

Initially, at elevated temperatures, we see a weak fluorescence pattern suggesting some spatial separation of dyes (Figure 4A). As the temperature is lowered, this pattern becomes gradually better-defined, culminating into a striking stripe pattern below the T_m (Figure 4B). A comparison with the bright-field image (Figure 4C) indicates that diI-C_{18} partitions preferentially within the grooves of the wrinkled ox-PDMS substrate, within the compliant membrane.

This temperature-dependent spatial separation of DiI-C_{18} within the periodically curved membrane environment suggests a simple model. Within the grooves of the wrinkled PDMS, the distal leaftlet of the conformal lipid bilayer must produce a denser molecular environment such as that preferred by diI-C_{18}. Moreover, this local increase in molecular densities within the grooves should elevate the

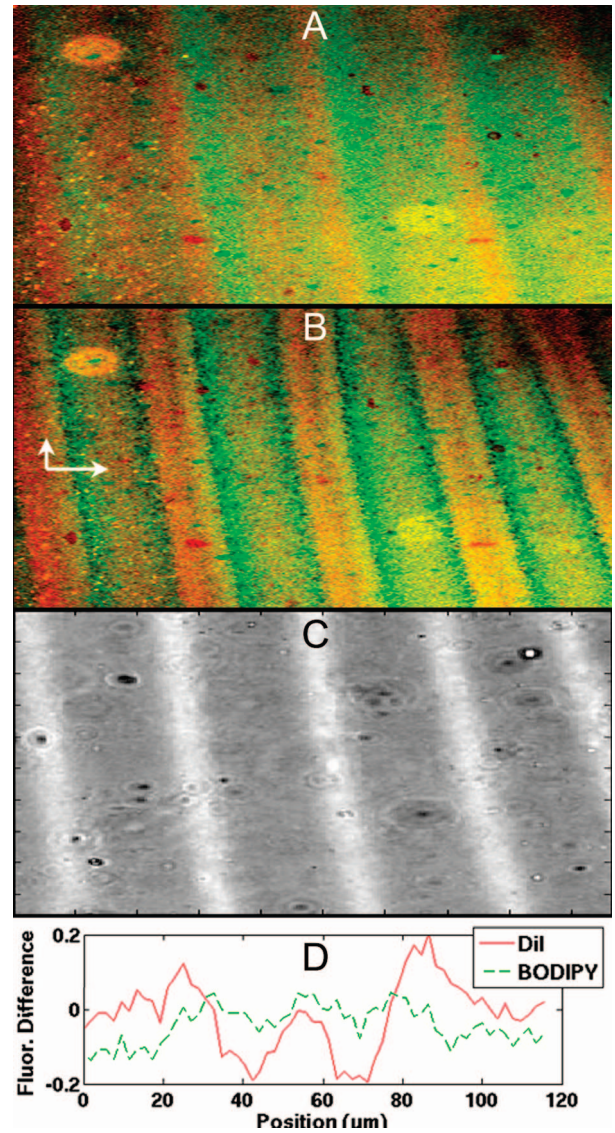

Figure 4. Curvature-dependent spatial reorganization and separation of membrane amphiphiles. Fluorescence images of a DMPC bilayer doped with 1 mol % C_{18}-diI and 3% BODIPY-FL-C12 deposited by vesicle fusion onto a wrinkled substrate. Red corresponds to diI excitation/emission, green to BODIPY-FL-C_{12}. (A,B) Images taken at 30 and 17.9 °C, respectively, above and below the DMPC phase transition temperature (T_m = 24.1 °C). The scale arrows indicate 50 μm, and the intensity range of each image channel is normalized to 3 standard deviations around the mean pixel value. (C) Bright-field image of the same region. (D) Spatial plot of redistributions in the normalized fluorescence intensities of the two dyes at 17.9 °C relative to 30 °C (after 466 s).

effective transition temperature for this region. As the temperature is lowered, the distal leaflet lipids within the grooves should gel first,[33] further attracting gel-preferring DiI-C_{18} that in turn enhances fluorescence intensity within the grooves. With subsequent cooling, the rest of the leaflet gels but the dye is entrapped by its immobile DMPC neighbors. The BODIPY-FL-C_{12} experiences less reorganization because of its relative indifference to local packing.

It is interesting to note that the widths of enhanced fluorescence (~10–20 μm) are considerably larger than the nanoscale roughnesses. The large width of the dye-enhanced regions (Figure 4B) with respect to the much smaller groove

width (Figure 1C) suggests long-range, possibly cooperative, effects on bilayer packing densities due to local perturbations. Such long-range effects are also observed in studies of lipid spreading, where the spreading fronts of lipid bilayers reveal laterally broad exponential dye intensity patterns[21] over tens of micrometers ascribed to local tension experienced by much narrower molecules at the bilayer edges. In sum, the simple experiment revealing curvature-dependent molecular reorganizations suggests that topology imposed by wrinkled elastomers can produce local differences in lipid organization (e.g., chain conformational order and packing density) and thus local transition temperatures.

Results described in this study show how wrinkled elastomers can impose complex three-dimensional topographies over large, macroscopic areas of adhering fluid lipid bilayers. Real-time variations in substrate topography prompt rapid shifts in membrane−substrate equilibrium, inducing both meso- and molecular-scale reorganizations. We anticipate future work leveraging this capability to conduct molecular-level investigations of curvature-dependent biophysical processes important to many cellular activities. Beyond biophysics, we envisage applications in sorting, separating, and fractionating membrane proteins and membrane-compatible amphiphilic molecules at solid surfaces.[34]

Acknowledgment. This letter combines work performed under a grant (DE-FG02-04ER46173) from U.S. Department of Energy's Biomolecular Materials Program. B.S. and A.M.S. are supported by fellowships from University of California's Graduate Research and Training Program in Adaptive Biotechnology (GREAT) and NSF Center for Biophotonics Science & Technology (CBST), respectively. We also gratefully acknowledge contributions and comments by A.W. Szmodis, G. McNerney, S. Sasaki, and the reviewers.

Supporting Information Available: Vesicle-fusion and lipid-spreading membrane deposition techniques; determining membrane morphology using dye-quenching experiments; detecting membrane topography using diffusion; FRAP technique; stretching apparatus; estimating maximum wrinkled curvature; video of the ellipse-fitting algorithm operation.

References

(1) Vogel, V.; Sheetz, M. *Nat. Rev. Mol. Cell Biol.* **2006**, *7*, 265–275.
(2) Zimmerberg, J.; Kozlov, M. M. *Nat. Rev. Mol. Cell Biol.* **2006**, *7*, 9–19.
(3) McMahon, H. T.; Gallop, J. L. *Nature* **2005**, *438*, 590–596.
(4) Seifert, U. *Adv. Phys.* **1997**, *46*, 13–137.
(5) Deuling, H. J.; Helfrich, W. *J. Phys.* **1976**, *37*, 1335–1345.
(6) Waugh, R. E. *Biophys. J.* **1982**, *38*, 29–37.
(7) Bacia, K.; Schwille, P.; Kurzchalia, T. *Proc. Natl. Acad. Sci. U.S.A.* **2005**, *102*, 3272–3277.
(8) Baumgart, T.; Hess, S. T.; Webb, W. W. *Nature* **2003**, *425*, 821–824.
(9) Groves, J. T. *Annu. Rev. Phys. Chem.* **2007**, *58*, 697–717.
(10) Parthasarathy, R.; Groves, J. T. *Soft Matter* **2007**, *3*, 24–33.
(11) Huang, J.; Juszkiewicz, M.; de Jeu, W. H.; Cerda, E.; Emrick, T.; Menon, N.; Russell, T. P. *Science* **2007**, *317*, 650–653.
(12) Efimenko, K.; Rackaitis, M.; Manias, E.; Vaziri, A.; Mahadevan, L.; Genzer, J. *Nat. Mater.* **2005**, *4*, 293–297.
(13) Cerda, E.; Mahadevan, L. *Phys. Rev. Lett.* **2003**, *90*.
(14) Bowden, N.; Huck, W. T. S.; Paul, K. E.; Whitesides, G. M. *Appl. Phys. Lett.* **1999**, *75*, 2557–2559.
(15) Chan, E. P.; Crosby, A. J. *Soft Matter* **2006**, xxx.
(16) Bowden, N.; Huck, W. T. S.; Paul, K. E.; Whitesides, G. M. *Appl. Phys. Lett.* **1999**, *75*, 2557.
(17) Sanii, B.; Parikh, A. N. *Annu. Rev. Phys. Chem.* **2008***59*May, http://dx.doi.org/10.1146/annurev.physchem.58.032806.104644.
(18) Efimenko, K.; Wallace, W. E.; Genzer, J. *J. Colloid Interface Sci.* **2002**, *254*, 306–315.
(19) Bowden, N.; Brittain, S.; Evans, A. G.; Hutchinson, J. W.; Whitesides, G. M. *Nature* **1998**, *393*, 146–149.
(20) Hovis, J. S.; Boxer, S. G. *Langmuir* **2000**, *16*, 894–897.
(21) Nissen, J.; Gritsch, S.; Wiegand, G.; Radler, J. O. *Eur. Phys. J. B* **1999**, *10*, 335–344.
(22) Axelrod, D.; Koppel, D. E.; Schlessinger, J.; Elson, E.; Webb, W. W. *Biophys. J.* **1976**, *16*, 1055–1069.
(23) Boxer, S. G. *Curr. Opin. Chem. Biol.* **2000**, *4*, 704–709.
(24) Lenz, P.; Ajo-Franklin, C. M.; Boxer, S. G. *Langmuir* **2004**, *20*, 11092–11099.
(25) Halir, R.; Flusser, J. In *Proceedings of the 6th International Conference in Central Europe on Computer Graphics, Visualization and Interactive Digital Media (WSCG98)*, Plzen, Czech Republic, 1998, pp 125–132..
(26) Swain, P. S.; Andelman, D. *Phys. Rev. E* **2001**, *63*, 51911.
(27) Helfrich, W. *Z. Naturforsch. C* **1973**, *28*, 693–703.
(28) Voeltz, G. K.; Prinz, W. A. *Nat. Rev. Mol. Cell Biol.* **2007**, *8*, 258–264.
(29) Huttner, W. B.; Zimmerberg, J. *Curr. Opin. Cell Biol.* **2001**, *13*, 478–484.
(30) Foster, M. C.; Yguerabide, J. *J. Membr. Biol.* **1979**, *45*, 125–146.
(31) Klausner, R. D.; Wolf, D. E. *Biochemistry* **1980**, *19*, 6199–6203.
(32) Spink, C. H.; Yeager, M. D.; Feigenson, G. W. *Biochim. Biophys. Acta* **1990**, *1023*, 25–33.
(33) We recall that several recent studies suggest that the two leaflets of supported lipid bilayers melt independently. These studies suggest that the lower leaflet experiences an enhanced stabilization due to substrate interactions, thus melting at higher temperatures (by several degrees) than the distal one.[34] Our model does not support nor dismiss the possibility that local curvature could enhance this effect, but we note that the lack of symmetry between the leaflets may explain why enhanced fluorescence in the distal leaflet is not fully countered by diminished fluorescence in the lower one.
(34) Feng, Z. V.; Spurlin, T. A.; Gewirth, A. A. *Biophys. J.* **2005**, *88*, 2154–2164.
(35) van Oudenaarden, A.; Boxer, S. G. *Science* **1999**, *285*, 1046–1048.
(36) Thomas, G. B.; Finney, R. L. *Calculus and Analytic Geometry*, 9th ed.; Addison-Wesley: Reading, MA, 1996.

NL073085B